JP1.2 THE NONLINEAR ENSO MODE AND ITS INTERDECADAL CHANGES

Aiming Wu and William W. Hsieh *
University of British Columbia, Vancouver, British Columbia, Canada

1. INTRODUCTION

In the mid 1970s, an abrupt change in SST and large-scale atmospheric circulation over North Pacific was observed (Trenberth 1990; Trenberth and Hurrell 1994). Following the climate shift, many aspects of El Niño notably changed (Wang 1995; Gu and Philander 1995; Wang and Wang 1996; An and Wang 2000). These changes were accompanied by a notable modification in the evolution pattern and spatial structure of the coupled ocean-atmospheric anomalies (Wallace et al. 1998). ENSO prediction skills of the coupled ocean-atmosphere models also exhibit some decadal dependence (Balmaseda et al. 1995; Kirtman and Schopf 1998).

Despite a number of hypotheses that have been recently proposed to explain the origin of the decadal variability in ENSO behavior (Gu and Philander 1997; Zhang et al. 1998; Kleeman et al. 1999; Barnett et al. 1999; Pierce et al. 2000), what caused the interdecadal changes of El Niño manner is a still subject of debate.

So far, linear methods are used to extract the couple mode from the climate data (Bretherton et al. 1992). A joint singular value decomposition (JSVD) was used to extract the dominant patterns derived for the 1961-75 and 1981-95 periods, respectively (Wang and An 2001). The maximum SST gradient and strongest zonal wind stress anomalies were all displaced eastward about 15 degrees longitude during 1981-95; similar result was mentioned by An and Wang (2000) using the SVD method.

Linear assumption implies that the patterns for the wind stress anomalies and SST anomalies during the warm states are strictly symmetric to those during the cold states and both the westerly and easterly anomalies will have an eastward displacement after 1980. However, the atmosphere-ocean coupled mode could be nonlinear. Recently, nonlinear canonical correlation analysis (NLCCA) method was developed via a neural network (NN) approach (Hsieh 2000). This method has been applied to study the relation between the tropical Pacific sea level pressure (SLP) and sea surface temperature (SST) by Hsieh (2001), where nonlinearity was found in both fields and the nonlinearity exhibited some interdecadal dependence.

In this work, NLCCA will be used to study the nonlinear air-sea interactions between the wind stress (WS) and the SST fields over the tropical Pacific at various lead/lag times. Also NLCCA will be applied to investigate the interdecadal changes of the ENSO mode by comparing the NLCCA modes before (1961-75) and after (1981-99) the Pacific climate shift. This work is organized as follows: In Section 2, the data and the method of NLCCA are briefly introduced. The NLCCA modes (based on the data for 1961-99) are described in Section 3. The leading NLCCA modes for the 1961-75 and 1981-99 periods were presented and compared in Section 4. Hybrid coupled models combining the NLCCA (or CCA) atmospheric models and an intermediate dynamic ocean model (Cane-Zebiak ocean model) were designed, with which the impact of the nonlinearity on ENSO properties (period) was discussed in Section 5. A summary and discussion are given in Section 6.

*Corresponding author address: William W. Hsieh, Dept. of Earth and Ocean Sciences, University of British Columbia, Vancouver, BC, Canada, V6T 1Z4; e-mail: whsieh@eos.ubc.ca

2. Methodology and data

2.1 NLCCA

Given two sets of variables **x** and **y**, canonical correlation analysis (CCA) is used to extract the correlated modes between **x** and **y** by looking for linear combinations

$$u = \mathbf{a}\cdot\mathbf{x} \quad \text{and} \quad v = \mathbf{b}\cdot\mathbf{y} \tag{1}$$

where the canonical variates u and v have maximum correlation, i.e. the weight vectors **a** and **b** are chosen such that the Pearson correlation coefficient between u and v is maximized (von Storch and Zwiers 1999).

In NLCCA, we follow the same procedure as in CCA, except that the linear combinations (from **x** to u, **y** to v) are replaced by nonlinear combinations using 2-layer feed-forward neural networks (NNs), which are represented by the double-barreled NN on the left hand side of Fig. 1. By minimizing the cost function $J = -\mathrm{cor}(u, v)$, one finds the parameters which maximize the correlation cor(u,v). After the forward mapping with the double-barreled NN has been solved, inverse mappings from the canonical variates u and v to the original variables, as represented by the two standard feed-forward NNs on the right side of Fig. 1, are to be solved, where the cost function J_1 is the mean square error (MSE) of the output $\mathbf{x}'$ relative to $\mathbf{x}$ (MSE**x**), and the cost function J_2, the MSE of the output $\mathbf{y}'$ relative to $\mathbf{y}$ (MSE**y**) are separately minimized to find the optimal parameters for these two NNs.

The nonlinear optimization was carried out with a quasi-Newton method. To avoid the local minima problem, an ensemble of 30 NNs with random initial weights and bias parameters was run. Also, 20% of the data was randomly selected as testing data and withheld from the training of the NNs. Runs where -cor(u,v), the MSE$\mathbf{x}$ or the MSE$\mathbf{y}$ for the testing dataset were 10% larger than those for the training dataset were rejected. The NNs

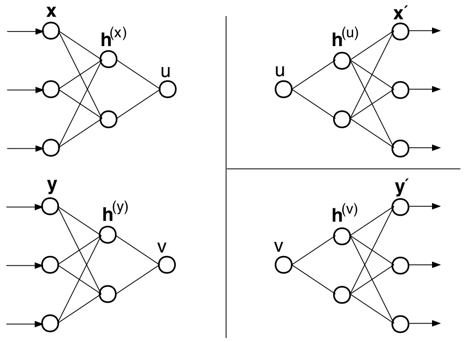

FIG. 1: A schematic diagram illustrating the three feed-forward neural networks (NN) used to perform the NLCCA model of Hsieh (2001). The double-barreled NN on the left maps from the inputs **x** and **y** to the canonical variates u and v. Starting from the left, there are l_1 input **x** va riables ('neurons' in NN jargon), denoted by circles. The information is then mapped to the next layer (to the right)— a 'hidden' layer $\mathbf{h}^{(x)}$ (with l_2 neurons). For input **y**, there are m_1 neurons, followed by a hidden layer $\mathbf{h}^{(y)}$ (with m_2 neurons). The mappings continue onto u and v. The cost function J forces the correlation between u and v to be maximized, and by optimizing J, the weights (i.e. parameters) of the NN are solved. On the right side, the top NN maps from u to a hidden layer $\mathbf{h}^{(u)}$ (with l_2 neurons), followed by the output layer $\mathbf{x}'$ (with l_1 neurons). The cost function J_1 minimizes the MSE($\mathbf{x}$), the mean square error of $\mathbf{x}'$ relative to **x**. The third NN maps from v to a hidden layer $\mathbf{h}^{(v)}$ (with m_2 neurons), followed by the output layer $\mathbf{y}'$ (with m_1 neurons). The cost function J_2 minimizes the MSE($\mathbf{y}$), the MSE of $\mathbf{y}'$ relative to **y**. When applied to the tropical Pacific, the **x** inputs were the first 5 PCs of the SST field, the **y** inputs, the first 5 PCs of the wind stress, and the number of hidden neurons were $l_2 = m_2 = 3$. An ensemble of 30 trials with random initial weights were run.

with the highest cor(u,v), and smallest MSE$\mathbf{x}$ and MSE$\mathbf{y}$ was selected as the desired solution.

2.2 *Data*

The monthly pseudo wind stress (WS) from the Florida State University (FSU) stress analyses (Shriver and O'Brien 1995) was used in this study. The data period is January 1961 through December 1999 covering the tropical Pacific from 124°E to 70°W, 29°S to 29°N with a grid of 2° by 2°. The monthly SST came from the reconstructed historical SST data sets by Smith et al. (1996) covering the period of January 1950 to December 2000 with a resolution of 2° by 2° over the global oceans. Monthly WS and SST anomalies were calculated by subtracting the climatological monthly means, which were based on 1961-99 period. The WS anomalies (for both zonal and meridional components) were smoothed by a 3-month running average. A linear detrending was then performed on both data.

Prior to NLCCA, traditional principal component analysis (PCA), also called empirical orthogonal function (EOF) analysis, was conducted on the WS and SST anomalies over the tropical Pacific (124°E-70°W, 21°S-21°N) to compress the data into manageable dimensions (Barnett and Preisendorfer 1987). For the WS, a combined EOF was applied to the zonal and meridional components of the WS anomalies (τ_x τ_y). Variance contributions from the 5 leading modes of WS are 15.4%, 9.8%, 6.0%, 5.2% and 3.7%, respectively, and for SST, 60.5%, 13.0%, 5.2%, 3.3% and 3.2%, respectively. The 5 leading principal components (PCs, i.e. the EOF time series) of WS and SST were used as the inputs to the NLCCA model.

3. The nonlinear ENSO mode extracted by NLCCA (based on 1961-99 period)

3.1 *NLCCA mode 1 with WS lagging SST*

Fig. 2 shows the NLCCA mode 1 solutions with WS lagging SST by 0, 3, 6, 9 and 12 months. Unlike the 5 curves for the SST modes (Fig. 2b), the 5 curves for the WS modes are dispersed (Fig. 2a), as are the CCA WS modes (Fig. 2c). Compared to the CCA modes, the curvature of the NLCCA modes varies with the lag time. The nonlinearity (i.e. curvature) is moderate at 0 month, very weak at 3 and 6 months, but increases at 9 and 12 months lag. Both the NLCCA and CCA modes rotate about 90° anticlockwise as lag varies from 0 to 12 months, indicating that the oscillations have changed from PC_1 dominated, to ones where PC_2 has an increasing role.

As the 5 curves for the SST modes are close to each other (Fig. 2b), the curvature of the NLCCA modes for the SST does not change much as the lag time varies, indicating that the nonlinearity in the SST is not dependent on the lag. The curves in Fig. 2b link the cool La Niña states on the left to the warm El Niño states in the lower right corner.

3.2 *NLCCA mode 1 with WS leading SST*

We interchange the roles of the predictor field and the response field between WS and SST by changing from WS lagging SST to WS leading the SST. Fig. 3 shows the first NLCCA modes with WS leading SST by 0, 3, 6, 9 and 12 months, as projected onto the PC_1-PC_2 planes. The curves of the WS modes at 0, 3 and 6-month lead are close to each other, but different from those for 9 and 12-month lead (Fig. 3a), which can also been seen in the corresponding CCA modes (Fig. 3c). The curves of the SST modes maintain a hump shape, getting increasingly curved as the lead increases from 0 to 12 months (Fig. 3b). The CCA SST modes also slightly rotate anticlockwise with lead time (Fig. 3d).

Therefore, at different lag/lead times, the correlated modes of both WS and SST are different, as manifested by the varying orientation of the CCA solutions (Figs. 2c,d and Figs. 3c,d), as well as the changing orientation and curvature of the NLCCA solutions. Generally, the NLCCA modes possess rotations similar to the CCA modes as

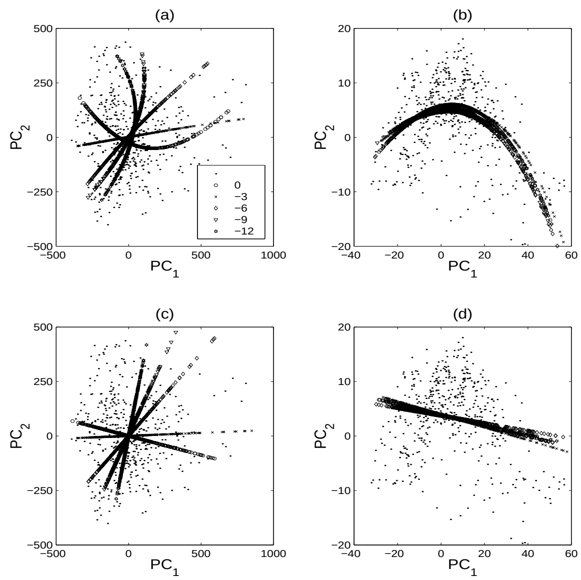

FIG. 2: The first NLCCA mode of the wind stress (WS) and SST anomalies projected onto the PC_1-PC_2 planes, as shown in panels (a) and (b), respectively. The data are denoted by dots, and the projected NLCCA solutions with WS lagging SST by 0, 3, 6, 9 and 12 months are denoted by the circle, cross, diamond, triangle and star, respectively. The corresponding CCA modes are shown in panels (c) and (d) for the WS and SST, respectively.

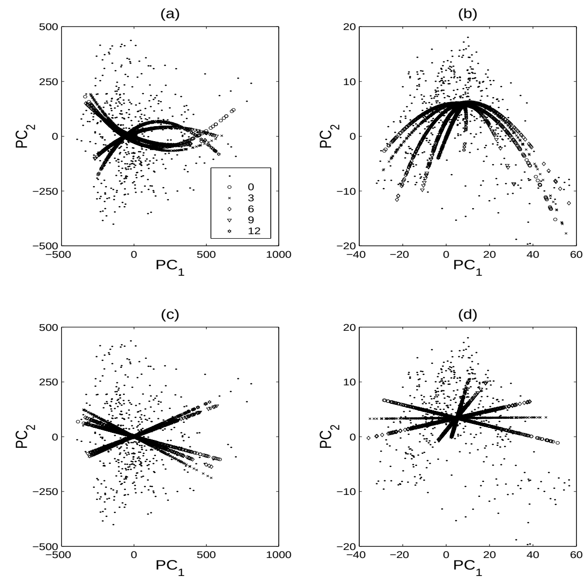

FIG. 3: Similar to Fig. 2 but with WS leading SST by 0, 3, 6, 9, and 12 months

the lag/lead time varies. The curvature and its variations in the NLCCA solutions indicates that the NLCCA modes for both WS and SST are generally nonlinear, with the degree of nonlinearity changing with the lag/lead time between the two variables.

3.3 *Spatial patterns of the NLCCA mode 1*

For a given value of the canonical variate u, one can map from u to the 5 PCs of the WS at the output layer (of the network in the top right corner of Fig. 1). Each of the PCs can be multiplied by its associated eigenvector (i.e. the EOF spatial pattern), and the 5 modes added together gives the spatial anomaly pattern for that value of u. The zonal WS anomalies corresponding to minimum u and maximum u for the NLCCA modes are shown in Fig. 4. Corresponding to minimum u, negative (easterly) anomalies appears over the central-western equatorial Pacific (Fig. 4a), slightly slanted towards the northwest-southeast direction, resembling the EOF1 pattern (not shown). Corresponding to maximum u, positive (westerly) anomalies dominates over the central-western equatorial Pacific (Fig. 4b). At lead times of 3-12 months (WS leading SST), the spatial patterns are similar to the EOF1, while at leads of 0 to -12 months, the westerly anomalies shift eastward, with easterly anomalies appearing over the northwestern equatorial Pacific, resembling the pattern of EOF3 (not shown), or more precisely, a combination of EOF1 and EOF3. As a result, the spatial patterns of WS anomalies are quite asymmetric on the opposite extremes of u, as the equatorial westerly anomalies (Fig. 4b) are further east than the equatorial easterly anomalies (Fig. 4a). The asymmetry is much more apparent when WS lags SST (the top 4 rows in Fig. 4), i.e., when WS is the response field. The zonal displacement between the positive center and the negative center reaches nearly 30° longitude. The magnitude of the westerly/easterly anomalies decreases rapidly with increasing lag time, but relatively slowly with increasing lead time—probably indicative of the relatively short 'memory' of the wind stress response to SST anomalies.

The WS spatial patterns for the CCA modes (not shown) shows some features similar to the NLCCA modes, e.g., the eastward shift of the equatorial anomalies as the lead time decreases. All anomaly patterns of the CCA modes for lead time from -6 to 12 months resemble the EOF1 pattern, despite the zonal shifts as the lead time varies. Furthermore, the spatial patterns on opposite extremes of u are completely symmetric, i.e. mirror images, though the amplitudes may differ by a constant at each lead time. Compared to the corresponding CCA modes, the westerly anomalies for the NLCCA modes are relatively stronger with their center located further east (Fig. 4b).

Similarly, anomaly patterns of SST associated with some specific values of v are calculated. Here the values of v are chosen at the time when u takes its minimum value or maximum value, For leads not exceeding 9 months, as WS shifts from extreme easterly anomalies to extreme westerly anomalies, the SST field varies from strong La Niña states to strong El Niño states. For the NLCCA modes (Fig. 5), the positive SST anomalies are basically distributed over the eastern equatorial Pacific, especially off the west coast of Southern America, while negative SST anomalies has various locations de-

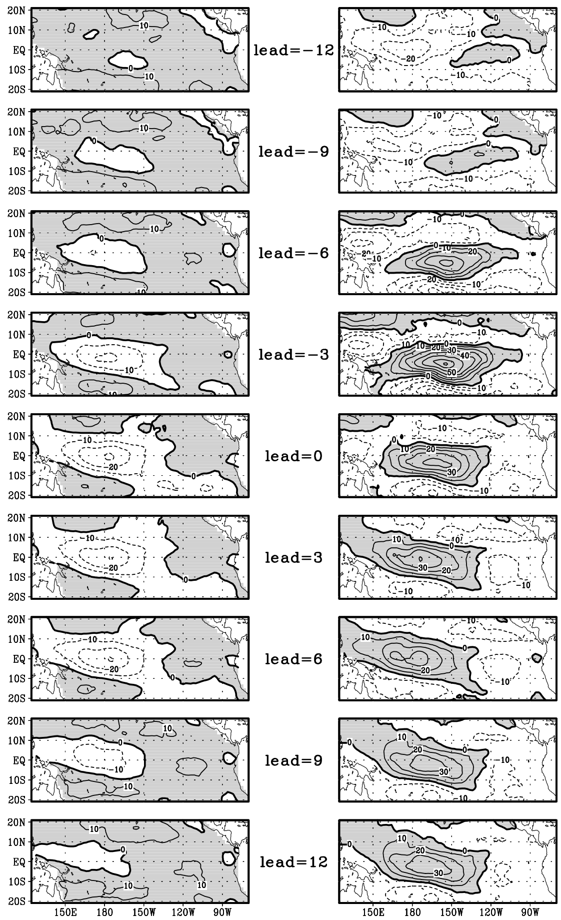

FIG. 4: The zonal WS anomaly patterns from the NLCCA mode 1 with the canonical variate u taking its minimum (left column) and maximum values (right column). From top to bottom, we have WS leading SST by $-12, -9, -6, -3, 0, 3, 6, 9$ and 12 months, with a negative lead time denoting a positive lag time. The contour interval is 10 m^2/s^2. Areas with positive values (westerly anomalies) are shaded.

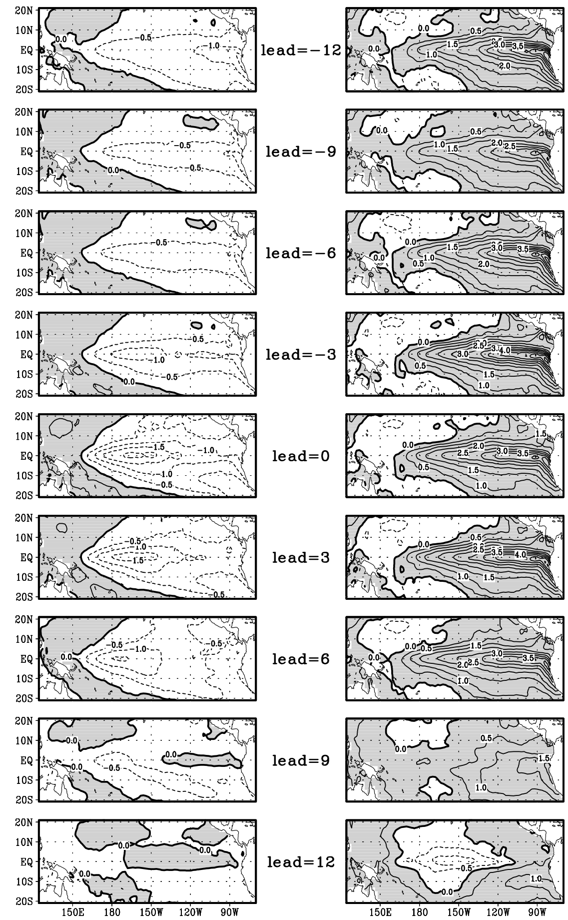

FIG. 5: Similar to Fig. 4, but for the spatial patterns of SST anomalies at the time when u takes its minimum and maximum values. Areas with positive anomalies are shaded. The contour interval is 0.5°C.

pending on the lead/lag times. When SST is a forcing field, i.e. WS lags SST in time, the negative SST anomalies appear over the eastern Pacific. As the lag time decreases and lead time increases (SST becomes the response field), the negative SST anomalies move to the central Pacific, illustrating the asymmetry between the La Niña states and the El Niño states. In Fig. 5b, at lead times of 9 and 12 months, the SST anomalies can no longer be accounted for mainly by EOF1, so higher EOF modes are needed. In general, Fig. 5 reveals that the spatial asymmetry between the two extremes of the oscillation is greater when SST is a response field (WS leading SST) than when SST is a predictor field (WS lagging SST).

In Figs. 2b and 3b, the large positive PC_1 values are accompanied by large negative values of PC_2, which gives stronger positive SST anomalies off Peru (Fig. 5b) than the CCA modes (not shown). Meanwhile, the large negative PC_1 values are accompanied by negative values of PC_2 in the NLCCA modes, resulting in weakened negative SST anomalies over the eastern Pacific and strengthened negative SST anomalies over the central Pacific (Fig. 5a), relative to the CCA modes. The CCA modes (not shown) give symmetric SST anomaly patterns for the La Niña and El Niño phases.

The mean square error (MSE) of the first NLCCA mode is less than that of the first CCA mode at all lead times from -12 to 12 months, for both WS and SST. Similarly, the explained variance by the first NLCCA mode is higher than that by the CCA mode at all lead times for WS and SST. The canonical correlation (i.e. the correlation between the canonical variates u and v) of the NLCCA mode is higher than that of the CCA mode, especially at longer lead/lag times. The ratio between the MSE of the NLCCA mode and that of the corresponding

CCA mode indicates how far the nonlinear mode deviates from the linear mode — the greater the nonlinearity, the smaller the ratio. This ratio varies with the lead time, and is generally smaller for the SST than for the WS, indicating greater nonlinearity in the SST.

4. Interdecadal changes of the nonlinear ENSO mode

4.1 *NLCCA mode 1*

The 5 leading PCs of the WS and SST were divided into 2 subsets: 1961-75 and 1981-99, upon which NLCCA was conducted separately. The solutions were projected onto the PC_1-PC_2 and PC_1-PC_3 planes (Fig. 6), where we can see that two curves representing the 1961-75 and 1981-99 epochs are similar to each other in the PC_1-PC_2 planes except that the SST curve for 1981-99 is slightly more curved (Fig. 6a) and that the WS curve extends further to the lower-right corner (Fig. 6b) relative to the curves for 1961-75. However, the two curves in the PC_1-PC_3 plane are quite different for both SST (Fig. 6c) and WS (Fig. 6d), with one approximately flipped to another along the PC_3, suggesting opposite contribution of EOF mode 3 to the NLCCA mode 1 during the 1961-75 and 1981-99 periods.

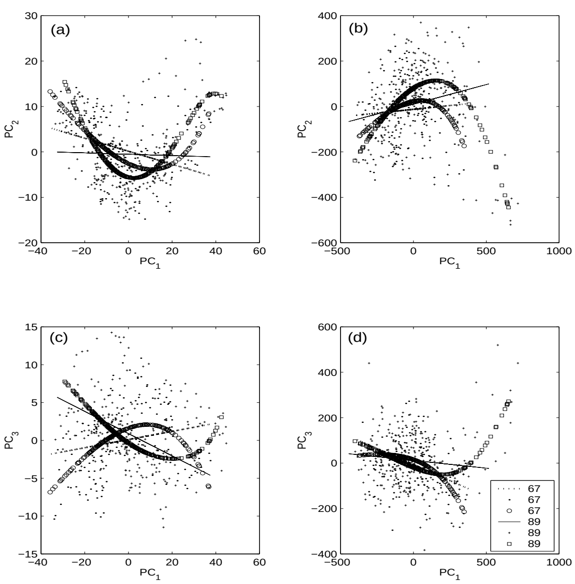

FIG. 6: The first NLCCA mode of the tropical Pacific SST (left column) and wind stress (WS) anomalies (right column) projected onto the PC_1-PC_2 planes shown in panels (a) and (b), and onto the PC_1-PC_3 planes shown in panels (c) and (d), respectively. The data for the period 1961-75 are denoted by dots, for the period 1981-99, by the symbol '+'. The projected NLCCA solutions for 1961-75 and 1981-99 are denoted by the circles and squares. respectively. The corresponding CCA mode 1 shown by the dashed line and solid line for the 1961-75 period and 1981-99 period, respectively.

By comparing with the corresponding CCA mode (shown by the dotted and solid lines in Fig. 6), the degree of the nonlinearity of the NLCCA mode was measured. The ratio of MSE between the NLCCA mode and the corresponding CCA mode is much smaller during 1981-99 than during 1961-75 for both SST and WS fields, and the increases of the canonical correlation and explained variance by the NLCCA mode relative to CCA mode are larger during 1981-99 than during 1961-75, indicating that the ENSO mode is more nonlinear after 1980.

4.2 *Spatial patterns of NLCCA mode 1*

For 1961-75, corresponding to maximum u, the SST field presents a fairly strong El Niño with positive anomalies (+2.0-2.5°C) over the central-eastern Pacific (Fig. 7c). Corresponding to minimum u, the SST field displays a La Niña with negative anomalies (about -2.0°C) over the central-western equatorial Pacific. The WS anomaly patterns corresponding to the same time as the SST anomalies in Fig. 7a and 7c occur present easterly and westerly anomalies over the central-western Pacific, respectively (see Fig. 7b and 7d), resembling the pattern of EOF1. Unlike the SST, the WS field does not exhibit apparent asymmetry, implying the WS during 1961-75 was nearly linear, though the SST displayed moderate nonlinearity.

For 1981-99, the SST anomaly patterns corresponding to minimum u and maximum u (shown in Fig. 7e and 7g) are similar to those for 1961-75 except that the asymmetry between El Niño and La Niña is enhanced. The positive anomalies exist further east off the South American coast, while negative anomalies extend further west over the central-western Pacific. Also the magnitude of the SST anomalies, particularly, the positive anomalies is increased (+3.0-3.5°C). Corresponding to minimum u, the WS field presents easterly anomalies over central-western equatorial Pacific resembling that for 1961-75 (Fig. 7b) with the amplitude somewhat strengthened. The WS field corresponding to maximum u displays further intensified westerly anomalies over the central Pacific (Fig. 7h), which exhibit an eastward shift about 30° longitude and a southward shift about 5° latitude relative to the easterly anomalies in Fig. 7f. Noting the easterly anomalies over the western equatorial Pacific, we can see that the pattern in Fig. 7h is actually a combination of patterns of WS EOF1, -EOF2 and EOF3. The asymmetry of the zonal WS structure between Fig. 7f and 7h indicates that the WS field is quite nonlinear during the 1981-99 period. Our results agree with Wang and An (2001), where a 15° longitude eastward displacement of WS anomalies was mentioned, which is exact an average of the patterns shown in Fig. 7f and 7h.

In Fig. 6a, on either curve, both large positive and negative SST PC_1 concurs with positive SST PC_2. In Fig. 6b, both large positive and negative WS PC_1 concurs with large negative WS PC_2. Considering the EOF1 and EOF2 of SST and WS (not shown), we can see this PC_1-PC_2 combination facilitates the asymmetry of SST and WS anomaly pattern illustrated in Fig. 7. Then why the WS had very weak nonlinearity during 1960-75 but

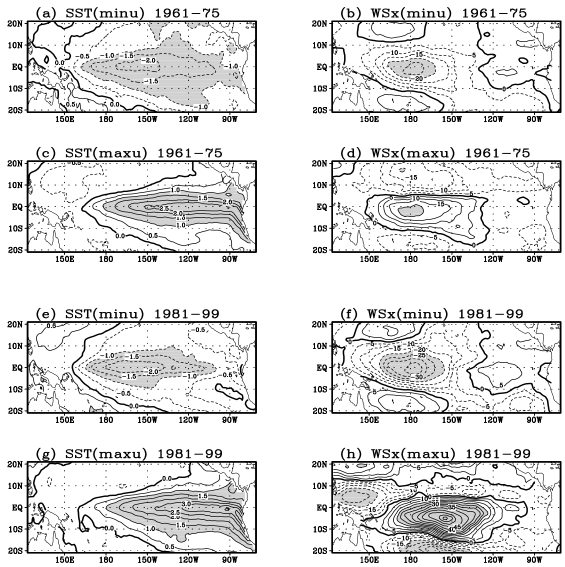

FIG. 7: The SST anomaly patterns (left column) and WS anomaly patterns (right column) from the NLCCA mode 1 when the canonical variate u taking its minimum (panels a, b, e and f) and maximum values (panels c, d, g, and h). The upper 4 panels represent the period 1961-75, and lower 4 panels, the period 1981-99. The contour interval is 0.5°C for the SST anomalies, and 5 m^2/s^2, for the WS anomalies. Areas where the SST anomalies are larger than +1°C or less than -1°C, or the WS anomalies are larger than +20m^2/s^2 or less than -20m^2/s^2 are shaded.

had considerable nonlinearity during 1981-99? The NLCCA curve for the 1981-99 WS (shown as squares in Fig. 6b) extends to larger negative PC_2 is one explanation. In addition, note that, in Fig. 6d, the two curves are flipped along the PC_3. For 1981-99, large positive WS PC_1 concurs with large positive PC_3 (upper-right corner), which facilitates eastward and southward shift of the westerly anomalies further intensifying the asymmetry generated by the nonlinear PC_1-PC_2 combination. However, for 1961-75, large positive WS PC_1 concurs with negative PC_3 (lower-right corner), which is unfavourable to the generation and enhancement of westerly anomalies over the eastern Pacific, i.e. prevents the nonlinearity occurring. The two curves are close to each other with small PC_3 values when PC_1 is negative (Fig. 6d), suggesting that the WS patterns (easterly anomalies) during La Niña states should be similar during 1961-75 and 1981-99, as can be seen in Fig. 7b and 7f.

In Fig. 6c, on the curve for 1981-99, large negative SST PC_1 concurs with large positive SST PC_3, which intensifies the negative anomalies over the central equatorial Pacific as over there is a negative anomaly in the SST EOF3, thus enhances the asymmetry of SST between El Niño and La Niña. In contrast, on the curve for 1961-75, large negative SST PC_1 concurs with large negative SST PC_3, which weakens the negative anomalies over the central equatorial Pacific, thus reduces the nonlinearity of SST.

Therefore, the difference of the nonlinear combination between PC_1 and PC_3 results in the interdecadal changes of the ENSO mode. Because the WS PC_3 has equivalent amplitude to the WS PC_2, while the PC_3 of SST is much weaker than the SST PC_2, the interdecadal changes in the WS are more significant than in the SST.

For the CCA mode 1 for either 1961-75 or 1981-99, the SST and WS anomaly patterns corresponding to minimum u and maximum u are completely symmetric (not shown). While the SST and WS anomaly patterns for CCA mode 1 during the 1961-75 period are similar to those during the 1981-99 roughly resembling to the patterns of EOF1, we still can see an eastward displacement of the anomaly patterns for 1981-99 relative to those for 1961-75, although the displacement is not as significant as that shown in Fig. 7. Also the SST or WS anomalies for 1981-99 are somewhat stronger than those for 1961-75.

5. Effects of the nonlinearity on ENSO period

5.1 *Delayed oscillator theory*

The dominant period of ENSO was increased from 2-3 years during the 1960s and 1970s to 4-5 years during the 1980s and 1990s (Wang and Wang 1996). One possible explanation for this is the eastward shift of the westerly anomalies after 1980 (An and Wang 2000; Wang and An 2001). Let us examine the consequences based on the delayed oscillator theory (Suarez and Schopf 1988): Let L be the width of the equatorial Pacific Ocean, and x the distance between the center of the westerly wind anomaly and the eastern boundary. If the wind anomaly appears at time $t = 0$, then warm SST appears at the eastern boundary at time $t_1 = x/c_K$, with c_K the eastward Kelvin wave speed. A cool Rossy wave also propagates westward at speed c_R for a distance of $L - x$ until it reflects at the western boundary as a cool eastward propagating Kelvin wave. The warming at the eastern boundary stops when the cool Kevin wave finally arrives at time $t_2 = (L - x)/c_R + L/c_K$. Hence the duration of warming at the eastern boundary is

$$T = t_2 - t_1 = (L - x)\left(\frac{1}{c_R} + \frac{1}{c_K}\right). \tag{2}$$

This implies that an eastward shift in the wind anomaly, i.e. a decrease in x, leads to an increase in T.

If x_A and x_B denote respectively the values of x before and after the climate shift, and T_A and T_B denote the corresponding durations of warming, then

$$\frac{\Delta T}{T_A} \equiv \frac{T_B - T_A}{T_A} = \frac{x_A - x_B}{L - x_A}. \tag{3}$$

If we assume the western boundary is at 124°E, and x_A is at the dateline, and $x_A - x_B$ to be 25°, then $\Delta T/T_A$ is 45%. Since the 25° shift in the westerly anomaly is based on the extreme of the NLCCA mode, while the average warm event may not reach the extreme, so an average shift may only be about 20°, which would still give a $\Delta T/T_A$ of 36%. We shall later see that these rough estimates for the fractional lengthening of the warm events as derived from the simple delayed oscillator theory actually agree quite well with the estimates from our hybrid coupled model and from observations.

For the linear JSVD, SVD or CCA results, the pattern of the easterly anomalies during the La Niña states is strictly symmetric to that of westerly anomalies during the El Niño states, i.e. the easterly anomaly fetch will occur over the same location where the westerly anomaly fetch takes place. Hence, the durations for both warm and cool events will be prolonged by the same amount, as can be seen in the wavelet diagram (An and Wang 2000, Fig. 1), where both positive and negative centers shift towards lower frequency after 1980.

However, our NLCCA results indicate that the coupled mode in the tropical Pacific could be nonlinear. The patterns for WS or SST anomalies could be very asymmetric, e.g. during the period 1981-99, only the westerly anomalies shifted eastward, while the easterly anomalies basically remained over the dateline. Thus, we argue that only the duration of warm events is prolonged, while that of cool events is unchanged.

Considering the Niño3.4 index calculated from the observed SST with the linear trend removed, we found that, during 1961-75, there were 76 warm months and 104 cool months, while during 1981-95, there were 105 warm months and 75 cool months. Here a warm (cool) month means the Niño3.4 index has a positive (negative) value at that time. Since there were 4 El Niño events during both periods (1963, 1966, 1969 and 1973; 1983, 1987, 1992 and 1995), this implies an increase in the average duration of warm events by 38% after 1980. For the Niño3 index, there were 62 warm months and 118 cool months during 1961-75, and 83 warm months and 97 cool months during 1981-99, with the average duration of warm events increased by 34% after 1980, approximately consistent with the estimates from the delayed oscillator theory.

5.2 ***Hybrid coupled model experiments***

Because of the limited sample size of the observed SST data, we will use a hybrid coupled model (HCM) to verify our results. The statistical atmospheric model is based on the first mode of the NLCCA or the CCA, which estimates the WS anomalies using the SST anomalies as predictors. The ocean model is basically that used in the Lamont model (Zebiak and Cane 1987). It is an anomaly model with the climatology of SST, currents, thermocline depth and background wind prescribed. The coupling procedure is as following: The SST anomalies from the ocean model are projected onto the eigenvectors of the observed SST anomalies yielding the 5 leading PCs of SST, which are served as the inputs to the NLCCA or CCA model. The outputs of the NLCCA or CCA model are the 5 PCs of the WS, which are multiplied by the corresponding eigenvectors to generate the WS anomalies. The WS anomalies are then used to force the ocean model to predict new SST anomalies. The above procedure is repeated until a desired integration is completed. Before running the couple model, the ocean model has been spun up with westerly anomalies for a certain time. It is worth pointing out that the FSU pseudo wind stress $\vec{\tau} = \vec{V} \cdot |\vec{V}|$ (with a unit of m^2/s^2) must be converted to real stress (with unit dyne) for coupling by multiplying it by a coefficient $\mu = \rho C_D$, where ρ is the air density and C_D is the drag coefficient. In the following coupled model experiments, μ may be considered as a coupling coefficient.

Based on the data for 1961-75 and 1981-99, 2 NLCCA models and 2 corresponding CCA models were built. Having the 4 statistical atmospheric models coupled with the ocean model, we consequently have 4 HCMs, named as HCM_{NL6175}, HCM_{NL8199}, HCM_{L6175} and HCM_{L8199}, respectively. Each HCM was run 250 years and the simulations for the last 150 years were used for analysis. Fig. 8 presents the Niño3 indices obtained from the last 50-year integrations by the 4 HCMs with a coupling coefficient μ = 0.05. The power spectrum analysis shows that the dominant periods for the simulated SST oscillations by HCM_{L6175}, HCM_{NL6175}, HCM_{L8199} and HCM_{NL8199} are 27.3, 24.0, 28.6 and 37.8 months, respectively. It is notable that the period is significantly increased by using HCM_{NL8199} (Fig. 8d), confirming that nonlinearity may prolong the ENSO period. In fact, because of the weak nonlinearity during 1961-75, the oscillation period from the HCM_{NL6175} has not increased relative to that of HCM_{L6175}.

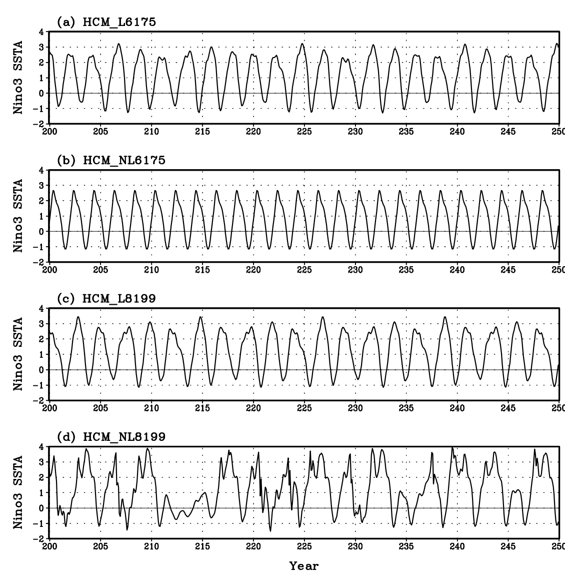

FIG. 8: Time series of the Niño3 SST anomalies simulated by 4 hybrid coupled models – HCM_{L6175}, HCM_{NL6175}, HCM_{L8199} and HCM_{NL8199}, as shown in panels a, b, c and d, respectively.

Contrast to the regular SST oscillations simulated by the other 3 HCMs, the HCM_{NL8199} presents an oscillation with considerable irregularity and somewhat enhanced amplitudes (up to +4°C) (Fig. 8d). The duration of the warm phases is apparently increased in Fig. 8d relative to other 3 panels, while the duration of cool phases remains basically unchanged. Therefore, the prolongation of the model ENSO period is mainly due to the increased duration of its warm phase.

6. Summary and discussions

The NLCCA model of Hsieh (2000, 2001) was applied to the surface wind stress and the sea surface temperature over the tropical Pacific. Nonlinearity can generally be detected in the NLCCA modes for both WS and SST, with the SST tending to be more nonlinear than the WS. The asymmetry between the warm El Niño states and cool La Niña states was well modelled by the first NLCCA mode, where westerly anomalies and positive SST anomalies are located further east than the easterly anomalies and negative SST anomalies, while the first CCA mode is incapable of modelling the spatial asymmetry. With the WS lagging and then leading the SST, we interchanged the roles of the predictor field and the response field between WS and SST. The spatial asymmetry is much more apparent in the response field than in the predictor field. Compared to the CCA modes, the NLCCA modes explain more variance of the two sets of variables and have higher canonical correlations, particularly at longer lead/lag time. The degree of nonlinearity varies with the lead/lag time between WS and SST.

Comparison of the nonlinearity of the coupled mode was made between the 1961-75 period and the 1981-99 period. From the leading NLCCA mode, we found notable interdecadal dependence in the nonlinearity of the coupled mode. During 1961-75, the WS showed no nonlinearity, while the SST revealed some nonlinearity. During 1981-99, the WS displayed fairly strong nonlinearity, and the nonlinearity in the SST was further enhanced. While nonlinearity can be detected between the EOF PC_1 and PC_2 as well as PC_1 and PC_3, the nonlinearity between PC_1 and PC_3 counteracts the nonlinearity between PC_1 and PC_2 in 1961-75, but reinforces the nonlinearity between PC_1 and PC_2 in 1981-99, resulting in greater nonlinearity during the 1981-99 period.

An advantage of the NLCCA over the CCA is that NLCCA is capable of presenting the asymmetry between the El Niño states and La Niña states. For the SST of both periods, negative anomalies during La Niña are centered further west of the positive anomalies during El Niño. The displacement is enhanced during 1981-99 as the main warming occurred even further east (off the South American coast). For the WS of the period 1961-75, the easterly anomaly patch during La Niña is basically symmetric to the westerly anomaly patch during El Niño with both centers located over the dateline. For the WS of the period 1981-99, the easterly anomalies during La Niña are intensified but unmoved, while the westerly anomalies during El Niño are shifted eastward by about 25° with increased amplitude. That the asymmetry between El Niño and La Niña was enhanced after 1980 (especially in the WS) suggests an increase in the nonlinearity of the ENSO mode.

The linearity of traditional CCA (or SVD) forces both westerly and easterly anomalies to shift eastward after 1980. According to the delayed oscillator theory, the ENSO period will increase as the duration for both the warm phase and that for the cool phase are prolonged. However, the NLCCA mode demonstrates that only the westerly anomalies shifted eastward after 1980. Thus we argue that the increase of the ENSO period after 1980 is mainly due to the prolongation of the warm phase. This was verified from the SST data, and further supported by numerical experiments with a hybrid coupled model (HCM), which combines the statistical atmospheric model (based on the NLCCA or CCA mode 1) and an intermediate dynamic ocean model (the Lamont ocean model).

In our HCMs for different decades, the annual climatological fields for the ocean model (e.g. the mean currents and upwelling) and the wind fields were kept unchanged, allowing us to focus on the changes of the anomaly mode. However, the changes in the climatological states may also lead to the changes in the ENSO propagation (Wang and An 2002). This explains why we did not see apparent interdecadal changes of ENSO propagation in our numerical experiments. In addition, only the first NLCCA mode was used in this study. More modes will be used for real-time prediction purposes.

Acknowledgements

This work was supported by research and strategic grants to W. W. Hsieh from the Natural Sciences and Engineering Research Council of Canada.

References

An, S.-I., and B. Wang, 2000: Interdecadal changes of the structure of the ENSO mode and its impact on the ENSO frequency. *J. Climate,* **13,** 2044-2055.

Balmaseda, M.A., K. Davet, and D.L.T. Anderson, 1995: Decadal and seasonal dependence of ENSO prediction skill. *J. Climate,* **8,** 2705-2715.

Barnett, T.P., and R. Preisendorfer, 1987: Origins and levels of monthly and seasonal forecast skill for United States surface air temperatures determined by canonical correlation analysis. *Mon. Wea. Rev.,* **115,** 1825-1850.

Barnett, T.P., D.W. Pierce, M. Latif, and D. Dommenget, 1999: Interdecadal interactions between the tropics and midlatitudes in the Pacific basin. *Geophy. Res. Lett.,* **26,** 615-618.

Bretherton, C.S., C. Smith, and J.M. Wallace, 1992: An intercomparison of methods for finding coupled patterns in climate data. *J. Climate,* **5,** 541-560.

Gu, D., and S.G.H. Philander, 1995: Secular changes of annual and interannual variability in the tropics during the past century. *J. Climate,* **8,** 864-876.

Gu, D., and S.G.H. Philander, 1997: Interdecadal climate fluctuations that depend on exchanges between the tropics and extratropics. *Science,* **275,** 805-807.

Hsieh, W.W., 2000: Nonlinear canonical correlation analysis by neural networks, *Neural Networks,* **13,** 1095-1105.

Hsieh, W.W., 2001: Nonlinear canonical correlation analysis of the tropical Pacific climate variability using a neural network approach, *J. Climate, 14,* 2528-2539.

Kirtman, B.P., and P.S. Schopf: 1998: Decadal variability in ENSO predictability and prediction. *J. Climate,* **11,** 2804-2822.

Kleeman, R., J.P. McCreary, and B.A. Klinger, 1999: A mechanism for generating ENSO decadal variability. *Geophy. Res. Lett.,* **26,** 1743-1746.

Latif, M., R. Kleeman, and C. Eckert, 1997: Greenhouse warming, decadal variability, or El Niño? An attempt to understand the anomalous 1990s. *J. Climate,* **10,** 2221-2239.

Pierce, D.W., T.P. Barnett, and M. Latif, 2000: Connections between the Pacific ocean tropics and midlatitudes on decadal time scales. *J. Climate,* **13,** 1173-1194.

Suarez, M.J., and P.S. Schopf, 1988: A delayed oscillator for ENSO. *J. Atmos. Sci.,* **45,** 3283-3287.

Shriver, J.F., and J.J. O'Brien, 1995: Low frequency variability of the equatorial Pacific ocean using a new pseudostress dataset: 1930-1989. *J. Climate,* **8,** 2762-2786.

Smith, T.M., R.W. Reynolds, R.E. Livezey, and D.C. Stokes, 1996: Reconstruction of historical sea surface temperatures using empirical orthogonal functions. *J. Climate,* **9,** 1403-1420.

Trenberth, K.E., 1990: Recent observed interdecadal climate changes in the Northern Hemisphere. *Bull. Amer. Meteor. Soc.,* **71,** 988-993.

Trenberth, K.E., and J.W. Hurrell, 1994: Decadal atmosphere-ocean variations in the Pacific. *Climate Dyn.,* **9,** 303-319.

Wallace, J.M., E.M. Rasmusson, T. Mitchell, V. Kousky, E. Sarachik, and Von H. Storch: 1998: On the structure and evolution of ENSO-related climate variability in the tropical Pacific: Lessons. *J. Geophy. Res.,* **103,** 14241-14259.

Wang, B., 1995: Interdecadal changes in El Niño onset in the last four decades. *J. Climate,* **8,** 267-285.

Wang, B., and Y. Wang, 1996: Temporal structure of the Southern Oscillation as revealed by waveform and wavelet analysis. *J. Climate,* **9,** 1586-1598.

Wang, B., and S.-I. An, 2001: Why the properties of El Niño changed during the late 1970s. *Geophy. Res. Lett.,* **28,** 3709-3712.

Wang, B., and S.-I. An, 2002: A mechanism for decadal changes of ENSO behavior: roles of backgroud wind changes. *Climate Dyn.,* **18,** 475-486.

Zhang, R.-H., L.M. Rothstein, and A.J. Busalacchi, 1998: Origin of upper ocean warming and El Niño change on decadal scales in the tropical Pacific Ocean. *Nature,* **391,** 879-883.

Zebiak, S.E., and M.A. Cane, 1987: A model El Niño-Southern Oscillation. *Mon. Wea. Rev.,* **115,** 2262-2278.

von Storch H, Zwiers FW (1999) *Statistical Analysis in Climate Research. Cambridge*, Cambridge Univ Pr 484 pp